

ArchesClimate: Probabilistic Decadal Ensemble Generation With Flow Matching

Graham Clyne^a, Guillaume Couairon^a, Guillaume Gastineau^b, Claire Monteleoni^{a,c}, Anastase Charantonis^a

^a *ARCHES, INRIA, Paris, France*, ^b *UMR LOCEAN, IPSL, Sorbonne Université, IRD, CNRS, MNHN, Paris, France*, ^c *Department of Computer Science, University of Colorado Boulder, USA*

arXiv:2509.15942v2 [physics.ao-ph] 28 Jan 2026

Corresponding author: Graham Clyne, clyne.graham@gmail.com

ABSTRACT: Climate projections have uncertainties related to components of the climate system and their interactions. A typical approach to quantifying these uncertainties is to use climate models to create ensembles of repeated simulations under different initial conditions. Due to the complexity of these simulations, generating such ensembles of projections is computationally expensive. In this work, we present ArchesClimate, a deep learning-based climate model emulator that aims to reduce this cost. ArchesClimate is trained on decadal hindcasts of the IPSL-CM6A-LR climate model at a spatial resolution of approximately 2.5×1.25 degrees. We train a flow matching model following ArchesWeatherGen (Couairon et al. 2024), which we adapt to predict near-term climate. Once trained, the model generates states at a one-month lead time and can be used to auto-regressively emulate climate model simulations. We show that for up to 10 years, these generations are stable and physically consistent. We also show that for several important climate variables, ArchesClimate generates simulations that are interchangeable with the IPSL model. This work suggests that climate model emulators could significantly reduce the cost of climate model simulations.

1. Introduction

Ensemble generation is an important tool to investigate the climate at any timescale. Given the chaotic nature of the atmospheric and ocean dynamics, small variations in initial conditions can evolve to vastly different states. As such, ensembles of climate model simulations can be seen as distributions of possible future climates. By repeatedly sampling the simulated climate, we enable probabilistic analyses that support the investigation of a broad range of problems, including extreme event attribution and uncertainty quantification (Fyfe et al. 2017; Fischer et al. 2023).

Furthermore, generating ensembles can significantly contribute to separating the internal variability from the effect of other sources of uncertainty, such as those associated with external forcings (Maher et al. 2021; Eade et al. 2014). Internal variability in climate models refers to the natural fluctuations in the climate system that occur without variations from external forcings (e.g. greenhouse gases or solar irradiation). These fluctuations arise from complex interactions between the atmosphere, ocean, land, and ice (e.g. El Niño or the North Atlantic Oscillation) — and can cause variations in climate at all time scales. Understanding internal variability improves confidence in detecting and projecting human-caused climate change.

Generating climate model ensembles traditionally requires perturbing initial conditions and running multiple resource-intensive instances of complex climate models (Deser et al. 2024). This practice is computationally expensive and severely limits the widespread generation of very large ensembles (Smith et al. 2019). To overcome this hurdle, significant research has focused on developing efficient atmospheric and coupled system emulators that can drastically reduce the associated computational cost.

Significant progress has been made in probabilistic climate emulation, notably with models like NeuralGCM (Kochkov et al. 2024). This model operates as a hybrid, physics-based, deep learning auto-regressive emulator, successfully generating temporally consistent atmospheric sequences. NeuralGCM captures robust variability by introducing the necessary randomness through the injection of noise directly into the neural network component of its hybrid architecture. Another approach is Spherical DYffusion (Cachay et al. 2023), a diffusion-based model explicitly designed as a probabilistic climate model emulator. This contrasts with the model cBottle, introduced by Brenowitz et al. (2025), a generative diffusion model that successfully learns the short-term, instantaneous dynamics of weather and climate when trained on multiple atmospheric

datasets, demonstrating the potential for generating realistic atmospheric states; however, its non-autoregressive design means it does not produce the long-term, temporally consistent sequences necessary for extended climate modeling. A major advance in auto-regressive climate modeling is seen in ACE and its successor, ACE2 (Watt-Meyer et al. (2024, 2023)). ACE2 is a deterministic emulator capable of generating stable sequential atmospheric states for up to 1000 years. However, its deterministic design may inherently underrepresent crucial internal variability, and its exclusive focus on the atmosphere omits the essential dynamics of the coupled ocean–atmosphere system. Additionally, the LUCIE framework (Guan et al. 2024) provides an approach aimed at efficiently learning and predicting components of the uncoupled system using ERA5 data. Addressing the need for a coupled approach, several models have emerged. DLESyM (Cresswell-Clay et al. 2025) is a complex coupled atmosphere-ocean emulator demonstrating the practical feasibility of simultaneously modeling the two major components trained with ERA5 data. The SamudrACE model (Duncan et al. 2025) complements this by combining the deterministic ocean model Samudra (Dheeshjith et al. 2025) with ACE2, resulting in a model that performs well and shows effective exchange between the ocean and atmosphere. Similarly, ACE-SOM2 (Clark et al. 2024) couples ACE2 with a simpler single-layer ocean model to investigate model response under different forcings, addressing generalization beyond stable climate scenarios.

Each of these approaches incorporates design decisions tailored to their specific objectives, but our goal is distinct: to efficiently emulate the IPSL-CM6A-LR at decadal timescales using probabilistic modeling across both oceanic and atmospheric domains in order to generate realistic ensemble members. We introduce ArchesClimate, an AI-driven probabilistic emulator that aims to learn climatic processes at a monthly temporal resolution. We adapted ArchesWeatherGen and trained it to emulate the IPSL-CM6A-LR model at approximately 2.5×1.25 degree resolution. We build on ArchesWeatherGen (Couairon et al. 2024), a state-of-the-art AI-based numerical weather prediction model, which is based on PanguWeather (Bi et al. 2022). ArchesWeatherGen provides a computationally efficient solution for ensemble generation that is adapted to climatic timescales.

We use a dataset from the Decadal Climate Prediction Project (DCPP), a Model-Intercomparison Project aimed at improving predictability and understanding climate at the decadal timescale (Boer et al. 2016). It comprises ensembles of 10 members with a duration of 10 years, starting every year between 1960 and 2015. This dataset provides us with many samples per year, which allows us to

efficiently learn the dynamics of IPSL-CM6A-LR over decadal scales. We use flow matching as our training scheme, a recent generative technique that learns a function to map one distribution to another distribution, usually from a multivariate normal distribution to the target data distribution (Lipman et al. 2023).

We target a monthly resolution to enhance the computational efficiency of the emulation process. This decision draws upon the theoretical framework that long-term system dynamics are driven by large-scale, low-frequency variability (Hasselmann 1976; Held et al. 2010). Therefore, we prioritize the representation of these slower modes by using a monthly timestep.

We distinguish between an emulator of the input/output functionality of the climate model versus an emulator of how a climate model evolves in climate state. The former describes a machine learning model that takes in boundary conditions or forcings and outputs full climate states, replacing the functionality of a climate model. The latter describes a machine learning model that learns dynamics from the output of a climate model, often augmenting the emulated climate model. In this research, we do the latter, and therefore our setting uses data from the IPSL-CM6A-LR for both initial conditions and training data. If we worked directly from the forcings and did not use an initial state generated from IPSL-6CMA-LR, we could instead attempt to replace the functioning of IPSL-6CMA-LR.

The manuscript is structured as follows: in section 2, subsection a and subsection b present the dataset and architecture used in the research, subsection d and subsection e outline how we train and generate data, and section 3 explains the experiments and their results. section 4 discusses conclusions and next steps.

2. Materials and Methods

a. Dataset

We use generated states from the IPSL-CM6A-LR coupled climate model (Boucher et al. 2020) submission to the DCPD (Boer et al. 2016). The DCPD aims at exploring decadal climate prediction, its predictability and variability. We use data from *hindcastA*, an experiment that performs 10-year hindcasts starting from 1960 to the present. Ensembles are initialized every year on January 1st from 1960-2015. For example, the dataset contains a 10-member ensemble from 1960-1970 and another 10-member ensemble for 1961-1971. While both these runs contain the years 1961-1970,

they will have their own internal variability and exhibit different dynamics. Therefore for any given initialization year, the 10-member ensemble resulting from this year will be different from the years produced by other initializations. This is an important element of this dataset, allowing us to learn the dynamics of the IPSL-CM6A-LR over a smaller timeframe with significantly more samples than in other MIP-style experiments. We use monthly outputs that are averaged values, corresponding to a dataset of approximately 70,000 simulated months. The 10 ensemble members have initial conditions generated by an assimilated run using observed sea surface temperature and sea surface salinity nudging over this period (Estella-Perez et al. 2020; Servonnat et al. 2015; Deser et al. 2024). Each ensemble member is forced with perturbed sea surface temperature and sea surface salinity. This perturbation is enough to generate variability in the ensemble while keeping some features leading to decadal predictability unchanged. We will refer to the dataset as IPSL-DCPP hereafter.

We select a subset of the available outputs of the IPSL-CM6A-LR, omitting a large portion of the available output. We choose not to account for the vertical structure of the ocean to reduce the size of the input state and instead use the ocean heat content that represents the vertically integrated heat at different depths. We use 10 surface variables, 7 oceanic variables and 7 atmospheric variables with 4 pressure levels (250, 500, 750, 800 hPa). As we are constrained computationally, we choose instead to use this subset of variables as a proof of concept to capture different climatic states at a monthly timescale.

The variables laid out in Table 1 capture important atmospheric and oceanic dynamics, including the heat and water flux between the two domains. The variables *net_flux* (total heat exchange between atmosphere and ocean, see A1 for a detailed description) and *evspsbl* (evaporation) represent the interactions between the two domains. The resolution of the atmospheric model is 144x143 (lon x lat, roughly 2.5x1.25 degrees), and the resolution of the ocean model is 362x332 (lon x lat, roughly 1 degree). The oceanic variables are re-gridded onto the regular atmospheric grid using a nearest-neighbour interpolation. For oceanic variables, we mask grid points over land with zeros. We also use the normalized, globally averaged atmospheric concentration of four greenhouse gases (*CO2*, *CH4*, *CFC11eq*, *N2O*) and solar irradiance from *input4mips*, a data repository of standardized boundary conditions used in model-intercomparison projects (Meinshausen and Nicholls 2018; Lurton et al. 2020).

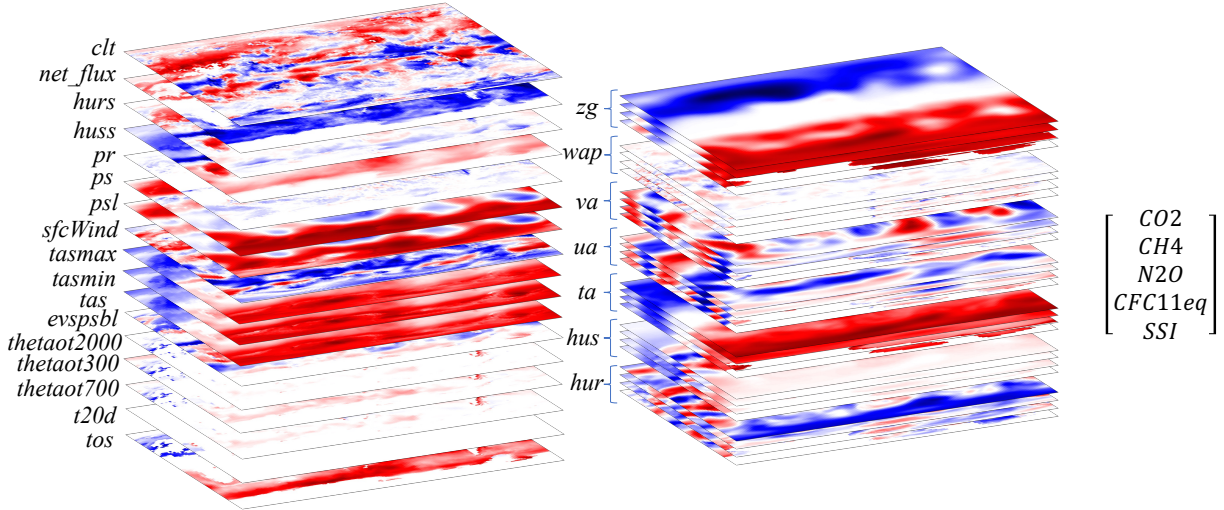


FIG. 1: On the right, a visualization of one state (X_t) from ISPL-DCPP, with surface and oceanic variables separated from atmospheric variables. Globally averaged and normalized external forcings are shown as a vector to the right.

b. Architecture

Here we describe the architecture of ArchesClimate. The backbone is very similar to ArchesWeatherGen, with the differences listed below (Couairon et al. 2024). The ArchesWeather architecture consists of a two-part machine learning system for weather forecasting: a deterministic model and a generative model. The deterministic component is built on a 3D Swin U-Net transformer structure based on PanguWeather and employs a novel Cross-Level Attention (CLA) mechanism to efficiently handle interactions across different vertical pressure levels (Bi et al. 2022; Liu et al. 2021; Vaswani et al. 2017). The second component, ArchesWeatherGen, is a probabilistic generative model that shares the same architecture and uses a flow matching approach to model the residual weather states, thereby enabling the generation of reliable ensemble forecasts to quantify uncertainty. This combined approach is designed to enhance both the accuracy of the deterministic prediction and the robustness of probabilistic forecasting while being computationally efficient. ArchesWeatherGen operates in a two-stage process to generate its forecasts. First, it uses an ensemble of deterministic models to calculate the most likely future atmospheric conditions, or the ensemble mean, for the next 6-hour timestep. Second, instead of generating a probabilistic forecast

TABLE 1: Variables in IPSL-DCPP

Variable Name	Long Name
Surface Variables	
<i>clt</i>	Total cloud cover percentage
<i>hurs</i>	Near-surface relative humidity
<i>huss</i>	Near-surface specific humidity
<i>pr</i>	Precipitation
<i>ps</i>	Surface air pressure
<i>tasmax</i>	Daily maximum near-surface air temperature
<i>tasmin</i>	Daily minimum near-surface air temperature
<i>tas</i>	Near-surface air temperature
<i>evspsbl</i>	Evaporation including sublimation and transpiration
<i>sfcWind</i>	Near-surface wind speed
<i>net_flux</i>	Total positive downward flux between ocean and atmosphere.
<i>psl</i>	Sea level pressure
Ocean Variables	
<i>thetaot2000</i>	Vertically-averaged potential temperature at 0-2000m
<i>thetaot700</i>	Vertically-averaged potential temperature at 0-700m
<i>thetaot300</i>	Vertically-averaged potential temperature at 0-300m
<i>t20d</i>	Depth of 20 degree celsius isotherm
<i>tos</i>	Sea surface temperature
Atmospheric Variables at 250, 500, 700, 850 hPa	
<i>hur</i>	Relative humidity
<i>hus</i>	Specific humidity
<i>ta</i>	Air temperature
<i>ua</i>	Eastward wind
<i>va</i>	Northward wind
<i>wap</i>	Omega
<i>zg</i>	Geopotential height
Forcings	
<i>CO2</i>	Atmospheric carbon dioxide (Yearly, Non-spatial)
<i>CH4</i>	Atmospheric methane (Yearly, Non-spatial)
<i>N2O</i>	Nitrous oxide (Yearly, Non-spatial)
<i>CFC12eq</i>	Trichlorofluoromethane (Yearly, Non-spatial)
<i>SSI</i>	Spectral solar irradiance (Daily, Non-Spatial)

of the entire next state, the model focuses its computational power on generating a probabilistic ensemble of residuals. The residual represents the difference between the predicted ensemble mean and the actual state. By focusing on predicting this residual, the model efficiently captures uncertainty and internal variability around the most likely forecast.

To extend the ArchesWeatherGen approach to the decadal climate prediction domain, we make the following changes:

- We include greenhouse gas and solar irradiance forcings using conditional layer normalization as done in Chen et al. (2021). The forcings listed in Table 1 are included as parameters.
- We remove axial attention to facilitate modeling of multiple domains. Axial attention breaks down attention into multiple 1D attentions along different axes (e.g., height and width separately for images). At the cost of increased complexity, we remove axial attention and attend to the flattened atmospheric layers, leaving it to the model to determine the relationship between each domain and its interactions (Ho et al. 2019).
- We increase the embedded dimension to 4 times the size of ArchesWeatherGen to account for this increased model complexity.
- We omit per-variable weighting in the loss function while keeping latitude weighting. Previous studies of weather emulators have included per-variable weighting (Bi et al. 2022), but given the different nature of our variable set, which contains ocean and atmospheric variables at a monthly timescale, we cannot reuse those weightings.

There are also changes to the training of ArchesClimate, which can be found in subsection d.

c. Forcings Included In ArchesClimate

To incorporate forcings in ArchesClimate, we adopt conditional layer normalization following (Chen et al. 2021). In this approach, each scalar forcing value is first passed through an embedding layer, which produces parameters that rescale and shift the outputs of a standard layer normalization. The forcings are CO_2 , CH_4 , $CFC11eq$, N_2O and SSI as described in Table 1. We apply conditional layer normalization in all transformer blocks of ArchesClimate, enabling the model to integrate conditioning signals at both global and local levels. By introducing greenhouse gas forcings through this mechanism, the model may be able to learn flexible relationships that adapt dynamically to

different forcing scenarios. This idea is explored in Appendix A2 but extensive investigation is left for further work.

d. Training

Following ArchesWeatherGen, we train both a deterministic and generative model to predict the next state at timestep $t + \delta$, where t is a timestep in IPSL-DCPP and δ is one month. A deterministic model, f_θ , is trained to predict $X_{t+\delta}$ from X_t where X is a climatic state of IPSL-DCPP (see 1). In this climate state, we include the forcings listed in Table 1 shown as Forcings_t in Figure 2. They are included in both f_θ and g_θ via conditional layer normalization (Chen et al. 2021). We then train a generative model g_θ to predict the residual of the predicted next state:

$$r_{t+\delta} = \frac{X_{t+\delta} - f_\theta(X_{t+\delta}|X_t, X_{t-\delta})}{\sigma} \quad (1)$$

where σ is the standard deviation of the residuals $(X_{t+\delta} - f_\theta(X_{t+\delta}|X_t, X_{t-\delta}))$ of the training dataset.

We use flow matching (FM) to train g_θ . FM takes known distribution p and finds a path of probabilities to an unknown distribution q (Lipman et al. 2023). This probability path is discretized over $S \in \mathbb{N}$ steps, where S denotes the total number of discrete time intervals used to approximate the continuous flow from p to q . In our case, p is the Gaussian distribution and q is the distribution of the residual of the IPSL-DCPP. Training involves learning θ such that g_θ predicts $r_{t+\delta}$. The inputs to g_θ are the predicted state of the deterministic model $f_\theta(X_t)$, the previous state $X_{t-\delta}$ and a residual noised according to a randomly chosen FM timestep $s \in S$, $(1-s)r_{t+\delta} + s\epsilon$, where ϵ is noise sampled from a Gaussian distribution. During training, we sample s from a standard normal distribution $s \sim \text{sigmoid}(\mathcal{N}(0, 1))$, and use the sigmoid function as done in Esser et al. (2024). See Figure 2 for a visualization of the process.

At each FM timestep s , the probability path is defined by a vector field that assigns a direction and magnitude to each point in our data to move between distributions. g_θ is updated to represent a vector field of the residual $(r_{t+\delta} - \epsilon)$ with the following loss function:

$$\mathcal{L} = \mathbb{E}_{s \in \mathcal{U}(0,1), \epsilon \in \mathcal{N}(0,1)} \left\| \left(g_\theta(X_t, f_\theta(X_{t+\delta}|X_t, X_{t-\delta}), \frac{(1-s)r_{t+\delta} + s\epsilon}{\sigma}) - (r_{t+\delta} - \epsilon) \right) \right\|_2^2 \quad (2)$$

We refer to (Lipman et al. 2023; Esser et al. 2024) for more details on the flow matching process.

We do not do out-of-distribution finetuning (training on data outside of the deterministic training dataset) as we have a distribution shift over time that needs to be captured in ArchesClimate. Finetuning could overfit to a particular temporal period.

The IPSL-DCPP dataset, which consists of 55 10-year, 10-member ensembles (one initialized annually), was carefully split to enable a direct comparison of full ensemble predictions with ArchesClimate. The split holds out 3 ensembles (initialized in 1989, 1999, and 2009) as the validation set and 8 ensembles (initialized in 1969, 1979, and 2010–2015) as the test set, leaving the remaining 44 ensembles for training. This configuration is justified by the ensembles’ distinct initial conditions, despite any temporal overlap, which allows for robust evaluation by comparing a complete 10-member ensemble from a given initialization year against the output of ArchesClimate. See A3 for a comparison of different train/test splits. We train the deterministic model for 10 hours on 4 A100 GPUs, and we train the probabilistic model for 20 hours on 4 A100 GPUs. See subsection f for a list of hyperparameters used.

e. Inference

Once both the deterministic and generative models are trained, ArchesClimate auto-regressively generates sequential states. To generate a state, the model needs to move from Gaussian noise ϵ to the data distribution of the following step. ArchesClimate takes $M \in \mathbb{N}$ FM steps during inference to go from $r_{t+\delta,0}$ to $r_{t+\delta,S}$ where M is a hyperparameter set at inference time. M is a small fraction of S . At each FM inference step s , the model outputs $r_{t+\delta,\Delta_{s+1}}$ with ArchesClimate until it reaches $r_{t+\delta,S}$ where Δ consists of evenly spaced values from 0 to S with a step size of $\frac{S}{M}$:

$$r_{t+\delta,\Delta_{s+1}} = r_{t+\delta,\Delta_s} + (\Delta_{s+1} - \Delta_s)g_\theta(r_{t+\delta,\Delta_s} | f_\theta(X_{t+\delta} | X_t, X_{t-\delta})) \quad (3)$$

Each step in the sampling process can be interpreted as taking a small step $(\Delta_{s+1} - \Delta_s)$ in the direction given by the vector field generated with g_θ , which is then added to the current state $r_{t+\delta,\Delta_s}$. To recreate $X_{t+\delta}$, we combine the output of the deterministic and generative model:

$$X_{t+\delta} = f_\theta(X_{t+\delta} | X_t, X_{t-\delta}) + r_{t+\delta,S} \quad (4)$$

Once ArchesClimate has followed the probability path to the data distribution, it can take $r_{t+\delta,S}$, the output from g_θ , and use Equation 4 to build the full next state. This is then passed to f_θ (and subsequently g_θ) as input to generate subsequent states. See Figure 3 for a visualization of this process. To initialize ArchesClimate for inference, the model begins with states taken from IPSL-DCPP. To generate states for the years 1969-1979, we will initialize ArchesClimate with January 1969 and February 1969 from a random ensemble member of IPSL-DCPP.

f. Training Details

TABLE 2: Hyperparameters used in ArchesClimate.

Hyperparameter	Value
Learning Rate	$4e^{-4}$
Inference Flow Matching Steps (M)	12
Training Flow Matching Steps (S)	1000
Optimizer	AdamW
Schedule	Cosine with Warmup
Warmup Steps	5000
Betas (β_1, β_2)	0.9, 0.98
Weight Decay	0.03

Quantifying the precise computational speedup of ArchesClimate relative to a traditional Earth System Model (ESM) like IPSL-CM6A-LR remains challenging due to fundamental differences in architecture and resolution. However, a rough comparison can be made by estimating the effective "parameter space" and normalizing for hardware differences.

The IPSL-CM6A-LR model operates on approximately 1.06×10^7 spatial grid points (Acosta et al. 2024). While the model tracks roughly 750 prognostic variables, the computational load is unevenly distributed. According to Acosta et al. (2024), the ocean component comprises the majority of the grid (9×10^6 points), compared to the atmospheric component (1×10^6 points). Assuming the computational load is dominated by standard ocean variables (approx. 41 variables based on CMIP6 "Omon" datasets), we estimate the effective parameter space of the IPSL model to be roughly 4.0×10^8 . In terms of throughput, IPSL-CM6A-LR completes 12 simulated years per day, consuming approximately 1,900 core-hours per simulated year (Acosta et al. 2024).

In contrast, ArchesClimate operates on a significantly reduced grid of $144 \times 144 \times 45$ (approx. 10^6 points). This suggests ArchesClimate is roughly 1/400th the size of the IPSL model in

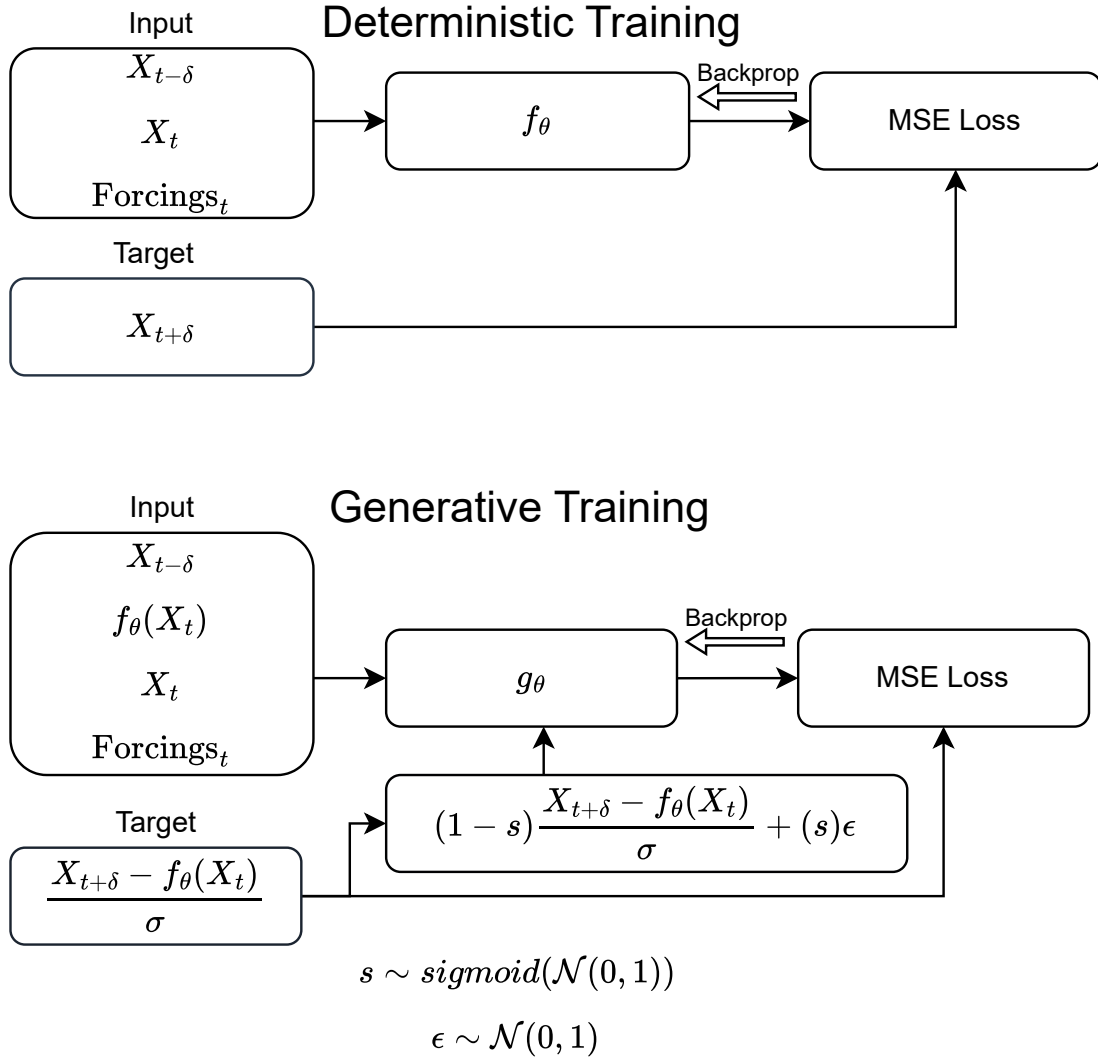


FIG. 2: Deterministic and Generative training schemes for ArchesClimate. It is necessary to have fully trained f_θ before training g_θ . f_θ learns a strong prior of the mean climate, while g_θ learns the residuals of the learned mean climate.

terms of spatial complexity. Furthermore, we assume here a monthly temporal resolution for ArchesClimate and IPSL, whereas in practice the IPSL model computes daily and hourly variables, further widening the computational gap.

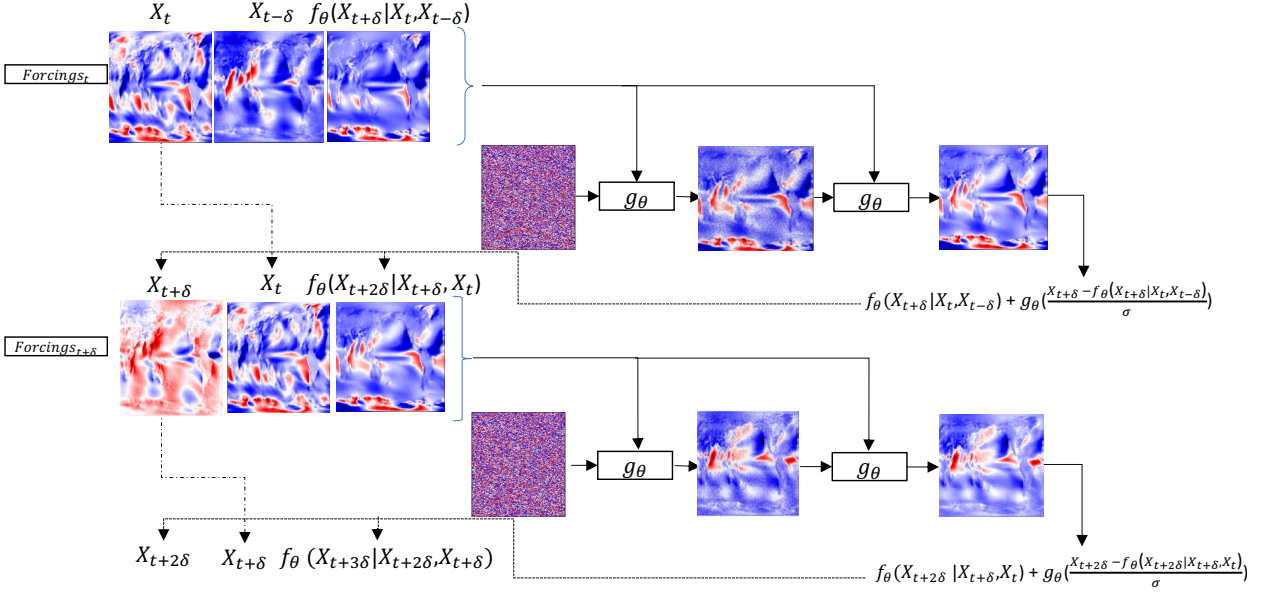


FIG. 3: Sampling with ArchesClimate. Initial states and noise are given to g_θ and slowly shift from noise to the data distribution over 24 inference timesteps. The combined result of f_θ and g_θ are then used as input for the following timestep t .

To compare costs, we must normalize the hardware usage. Using the approximation that one NVIDIA V100 GPU is roughly equivalent to 200 CPU cores (Kim et al. 2021), we can derive a “core-hour” equivalent for the machine learning model. ArchesClimate simulates 10 years in 12 minutes, or 50 simulated years per wall-clock hour. Using the conversion factor of 200 cores, 1 hour of GPU time equals 200 core-hours. Therefore, $200/50$ results in a cost of 4 core-hours per simulated year for ArchesClimate.

While ArchesClimate is drastically cheaper in absolute terms (4 vs. 1,900 core-hours), this efficiency is largely a function of its reduced resolution. If we were to scale ArchesClimate linearly to match the IPSL’s parameter space (multiplying the cost by the size factor of 400), the theoretical cost would rise to 1,600 core-hours per simulated year. This implies that at equivalent resolutions, the ML approach might be only marginally less expensive than the physics-based GCM. Moreover, if higher temporal resolutions were required, the ML cost could exceed that of the GCM. However, linear scaling may be an overly pessimistic assumption, as ML techniques often leverage latent spaces to improve efficiency beyond brute-force scaling. The primary value of ArchesClimate is not necessarily raw per-parameter efficiency, but its ability to approximate IPSL dynamics—effectively distilling a complex model—without running the full simulation. The IPSL is not capable of doing

reduced-complexity runs, and our technique to distill the model’s dynamics enables this reduced-complexity. Finally, total cost comparisons must account for training overhead, a factor often omitted in GCM estimates. The deterministic ArchesClimate model required 20 hours of training on 8 V100s, while the generative model required 20 hours on 4 A100s. Both physics-based and ML models require extensive tuning, adding further complexity to a direct “price tag” comparison.

3. Experiments

In this section, we describe the setup, evaluation methods and diagnostic tools used in experiments conducted with ArchesClimate. We then describe each experiment and its results.

a. Baselines

To measure how well ArchesClimate captures the dynamics of IPSL-DCPP, we consider the following baselines.

Held-out IPSL-DCPP Ensemble For each target ensemble, we select 5 members of the 10 members to serve as a baseline. We then compare both the remaining 5 ensemble members of IPSL-DCPP and a 5-member ArchesClimate ensemble to the baseline.

Pattern Scaling Baseline Following ClimateBench (Watson-Parris et al. 2022), we employ the Pattern Scaling method. Pattern scaling is a computationally efficient technique that estimates detailed regional climate changes for various future scenarios by simply multiplying a fixed spatial map of change (derived from complex models) by the projected global average temperature. Pattern scaling is known to be an effective means to predict spatial temperatures, but struggles with learning non-linear relationships such as precipitation (Tebaldi and Arblaster 2014). We train a linear regression model using global-mean temperature to predict these spatially explicit means. Consistent with the ClimateBench framework, we provide the global mean temperature as input (Watson-Parris et al. 2022). We provide the pattern scaling method with the monthly global mean. We train the linear regression model with the same data used in ArchesClimate. We generate an ensemble by using the global mean temperature from each ensemble member in IPSL-DCPP. We use the resulting generated states to compare the CRPS and Variance with ArchesClimate and IPSL-DCPP.

An alternative approach is to use climatology as a baseline, i.e. the monthly mean averaged over the training set; however, we found that climatology provided no useful signal. After approximately one year, climatology performed better than the held-out 5-member ensemble on variables with little to no climatic trend, but performed worse for variables with a discernible trend. As such, we opted for the more informative baseline described above.

b. Evaluation Metrics and Diagnostic Tools

Continuous Ranked Probability Score (CRPS) is a metric used to evaluate the accuracy of probabilistic forecasts by measuring the difference between the predicted cumulative distribution function and the observed outcome. We use the same implementation of CRPS as in Rasp et al. (2024) and is latitude-weighted.

Rank Histograms are a diagnostic tool used to evaluate the consistency or calibration of an ensemble forecast by comparing it to another ensemble (Hamill 2001). Using rank histograms, we evaluate whether an ensemble member generated with ArchesClimate can be interchanged with any member of the IPSL-DCPP ensemble. To calculate the rank of an ensemble member, we take the pixel-by-pixel values of the ensemble member and compare them to a target ensemble. We calculate the rank of the pixel value of the ensemble member compared to the rest of the target ensemble members at that pixel. We then take an average of the rank of each pixel across space and time. The histograms show the normalized frequency of the emulated ensemble member at that rank. We normalize the frequency by taking the mean and standard deviation of all frequencies across space and time. If the generated ensemble member can be interchanged with any member of an IPSL-DCPP ensemble, the histogram will be flat, showing an even distribution across all ranks.

Temporal Power Spectra (TPS) describes how the variance (or power) of a signal that changes with time is distributed among components that oscillate at specific rates (temporal frequencies, measured in cycles per unit time). This shows the strength of signals at varying timescales. We compute the TPS by calculating the temporal Fourier transform of the time series at each spatial location. We then take the positive frequencies and average spatially. We formalize this definition below:

Given a pixel at $x(\text{time, lat, lon})$ with $T := 120$ months (10 years),

$$\text{lat} = 1, \dots, N_y, \quad \text{lon} = 1, \dots, N_x, \quad \mathcal{K} = \left\{ k \mid 1 \leq k \leq \left\lfloor \frac{T}{2} \right\rfloor = 60 \right\}$$

$$X(k, \text{lat}, \text{lon}) = \sum_{n=0}^{119} x(n, \text{lat}, \text{lon}) e^{-i2\pi kn/120} \quad (5)$$

$$\overline{\text{PSD}}(k) = \frac{1}{N_x N_y} \sum_{\text{lat}=1}^{N_y} \sum_{\text{lon}=1}^{N_x} |X(k, \text{lat}, \text{lon})|, \quad k \in \mathcal{K} \quad (6)$$

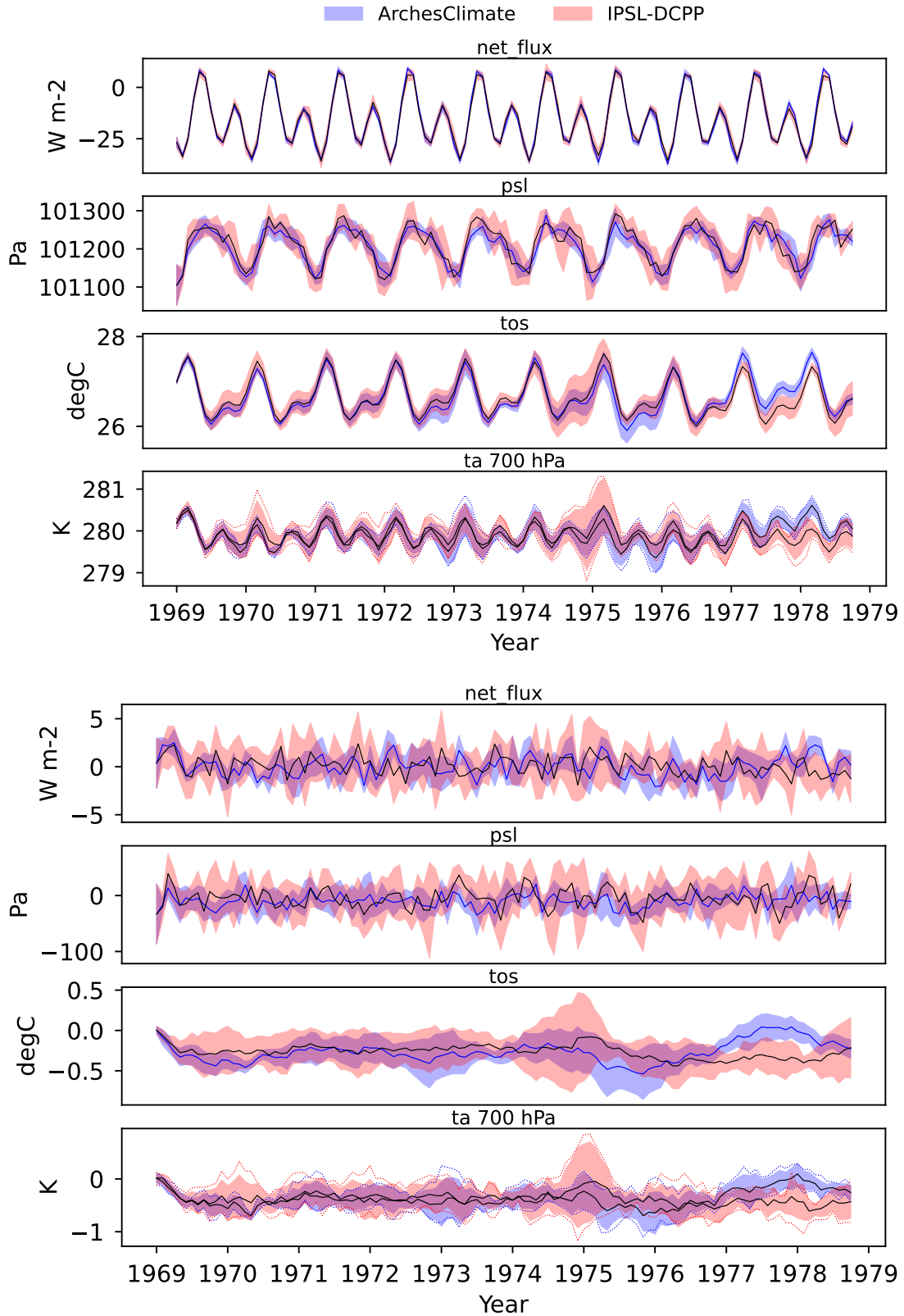


FIG. 4: Ensemble means of the full state (top) and ensemble means for anomalies (bottom) of the Tropics (20° S – 20° N, 0° – 360° E) for the test period 1969-1979. The dotted lines are the maximum and minimums for each 5-member ensemble mean, with the shaded area being +/- 1 standard deviation. Closer to the dotted line is better.

c. Regional Accuracy of ArchesClimate in the Tropics

By training on the full state of a given timestep, ArchesClimate can learn both the signal for the seasonal cycle and the anomaly, both of which are important aspects of decadal climate analysis (Smith et al. 2019). The seasonal cycle is the predictable annual pattern of changes caused by Earth’s position around the Sun, while anomalies are deviations from this expected seasonal average. Looking at anomalies is important in climate science because they highlight changes relative to a long-term average, making it easier to detect trends and patterns beyond natural variability. In this experiment, we qualitatively compare the performance of ArchesClimate to IPSL-DCPP in the Tropics (20°S–20°N, 0°–360°E) for both the full state and the anomaly of the full state. We use ArchesClimate to generate a 10-member ensemble and compare it to a 10-member ensemble of IPSL-DCPP for the test period initialized at 1969 for the Tropics. Each ensemble is 120 months (10 years), and we assess the stability and the regional accuracy of the generated states from ArchesClimate. We target the Tropics as they exhibit many important dynamics at climatic timescales (Wang 2019). To show the performance in both ocean and atmosphere, we select a subset of variables emulated in ArchesClimate. Sea surface temperature (*tos*) and sea level pressure (*psl*) exemplify ocean dynamics, while total positive downward flux (*net_flux*) shows interactions between atmosphere and ocean. Air temperature (*ta*) at 700 hPa provides an example of atmospheric dynamics.

In Figure 4, ArchesClimate captures the seasonal cycle across the selected variables. When the seasonal cycle is removed, we can see that ArchesClimate produces anomalies similar to IPSL-DCPP. There are small deviations between ArchesClimate and IPSL-DCPP at the end of the 10 years in the temperature variables *tos* and *ta*, and significant variance around 1975 in IPSL-DCPP that is not present in ArchesClimate. As each ensemble member is auto-regressively generated, internal variability will be present in each ensemble member, providing deviations from IPSL-DCPP. ArchesClimate generated stable states for the 10-year period of the experiment and accurate anomalies of these stable states for the variables presented.

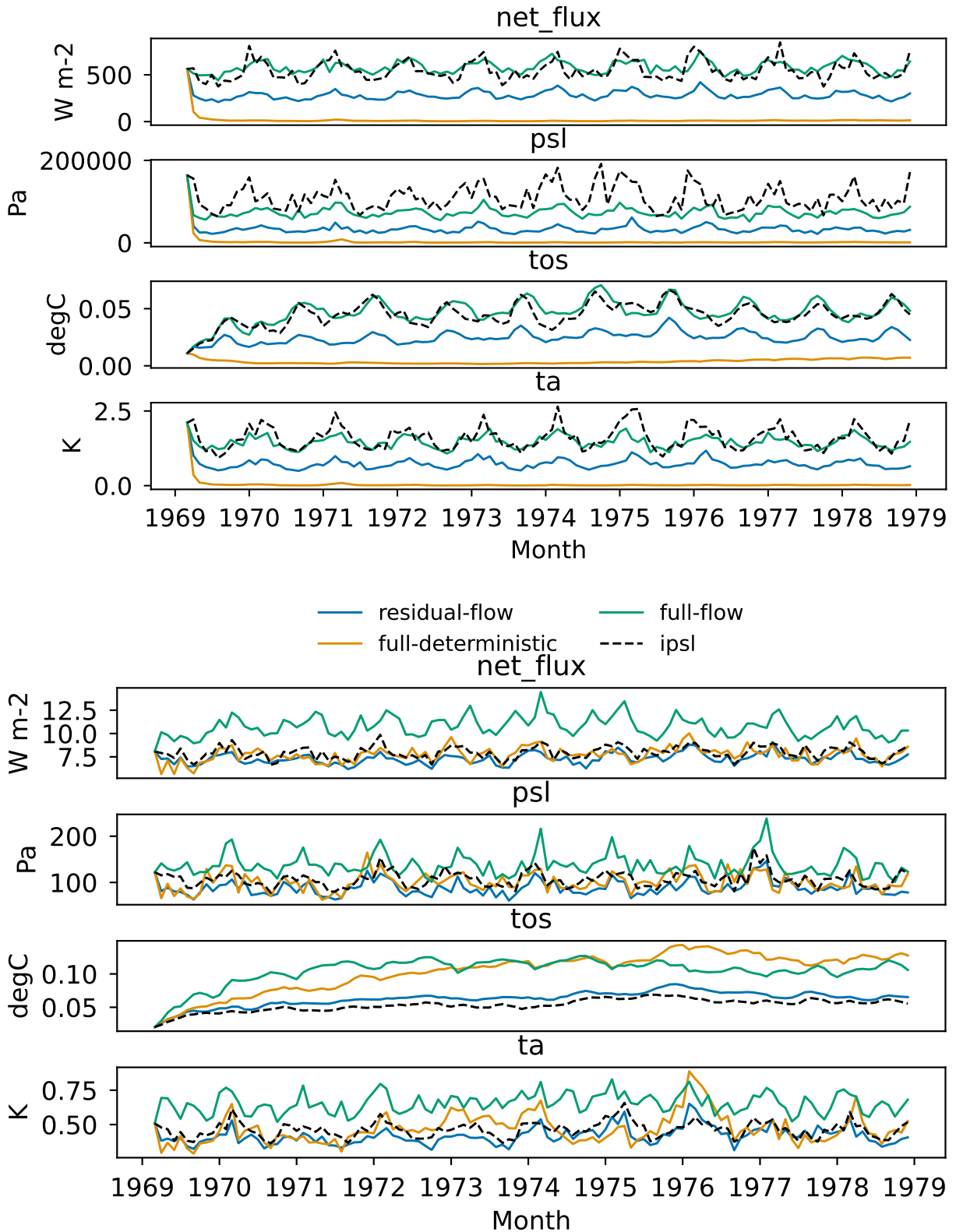


FIG. 5: Variance (top) and CRPS (bottom) for different training schemes for the decade 1969-1979. *residual-flow* is described in subsection d. *full-flow* trains without any deterministic model. *full-deterministic* uses only the deterministic model to make predictions. The dotted line represents the 5-member IPSL-DCPP baseline.

d. Comparison of Training Schemes

ArchesClimate uses a combination of deterministic and generative models. To assess the training scheme outlined in subsection d (hereby referred to as *residual-flow*), we compare it to several other schemes. We make predictions using only a deterministic model and only a probabilistic model, named *full-deterministic* and *full-flow*, respectively. We compare these methods to our pattern scaling baseline outlined in subsection a.

We see in Figure 5 that *full-deterministic* exhibits low variance compared to the other methods. *Full-flow* has similar variance to IPSL-DCPP but is less accurate than residual-flow across all variables. By combining the probabilistic and deterministic components (as shown in *residual-flow*), ArchesClimate makes much more accurate predictions and generates more variance than *full-deterministic*. We can see in *tos* that both *full-deterministic* and *full-flow* have high CRPS scores compared to IPSL-DCPP, but *residual-flow* has a similar CRPS score to IPSL-DCPP. The probabilistic model, when trained in tandem with the deterministic model, provides error correction and improves accuracy on top of increasing variance. We investigate methods to increase the variance of *residual-flow* in subsection j. We outperform the pattern scaling baseline across all metrics, with the exception of temperature variance. While the numerical margin is small, this performance is notable given the methodological differences: the baseline is conditioned on perfect global mean temperatures for every month, whereas ArchesClimate performs a fully autoregressive rollout over the 10-year period. By using pattern matching for temperature, variance in ArchesClimate could potentially be improved. This exploration is left for further work.

e. CRPS and Standard Deviation of ArchesClimate

We assess how the model responds to varying forcings and initializations by computing the average Continuous Ranked Probability Score (CRPS) and standard deviation over three distinct periods: 1969–1979, 1979–1989, and 2010–2020. To evaluate a wider range of dynamics, we expanded the variable subset used in subsection c to include vertically-averaged potential temperature at 0–2000m (*thetaot2000*), vertical velocity (*wap*), geopotential (*zg*), and relative humidity (*hur*). The pattern scaling baseline is derived from the monthly global mean temperature of each ensemble member, allowing us to generate a full ensemble for comparison. Further details on these metrics are provided in subsection b.

As shown in Table 3, ArchesClimate achieves a lower CRPS than IPSL-DCPP for all variables except θ_{2000} . However, the standard deviation is consistently higher in the IPSL-DCPP reference across all periods. Because ArchesClimate predicts the mean state deterministically and residuals probabilistically, the variance can be adjusted by increasing the initial noise amplitude during residual generation—a topic explored in subsection j.

The interpretation of these scores requires nuance. A CRPS lower than the IPSL score indicates that ArchesClimate captures the distribution of the target IPSL-DCPP members more effectively than the internal IPSL-DCPP ensemble members do among themselves. Since our goal is to faithfully emulate the original model’s dynamics, a lower CRPS is not inherently better; rather, we aim for a score similar to that of the IPSL-DCPP baseline. This metric ambiguity necessitates the qualitative analysis of generated states conducted in subsequent experiments.

Finally, while the pattern scaling baseline yields a similar CRPS, it exhibits significantly lower variance than both IPSL-DCPP and ArchesClimate. This result is expected, as pattern scaling predicts values near the ensemble mean. Furthermore, unlike ArchesClimate, pattern scaling is not auto-regressive and is provided with the ground-truth global monthly means as input.

Variable	CRPS			Std. Dev.		
	ArchesClimate	IPSL-DCPP	Pattern Scaling	ArchesClimate	IPSL-DCPP	Pattern Scaling
θ_{2000} (°C)	0.06	0.05	0.04	0.14	0.22	0.03
t_{os} (°C)	0.27	0.27	0.18	0.51	0.71	0.01
p_{sl} (Pa)	87.98	106.39	95.18	174.73	330.18	8.3
net_flux (W/m ²)	7.25	7.97	7.27	16.44	23.33	0.6
z_g 700 hPa (m)	8.38	10.03	9.32	15.57	30.63	2.7
wap 700 hPa (Pa/s-1)	1.07e-02	1.14e-02	1.00e-3	2.56e-02	3.11e-02	6.71e-04
t_a 700 hPa (K)	0.41	0.46	0.44	0.82	1.26	0.25
hur 700 hPa (%)	2.78	3.02	2.57	5.69	7.44	0.27

TABLE 3: Comparison of CRPS and Standard Deviation between ArchesClimate, IPSL-DCPP and Pattern Scaling. Scores are averaged over space and time for three test periods: 1969-1979, 1979-1989 and 2010-2020. Both metrics keep the units shown in the table. All stats are generated from 5-member ensembles and are compared against a held-out 5-member ensemble from IPSL-DCPP. Closer to IPSL-DCPP is better.

f. Interchangeability using Rank Histograms

To evaluate whether ensemble members generated by ArchesClimate are exchangeable with those of IPSL-DCPP, we conducted a rank histogram analysis. We compared a 10-member

ArchesClimate ensemble against a 10-member IPSL-DCPP ensemble, both initialized in 1969, over a 10-year period in the North Atlantic (0° – 65° N, 80° – 0° W). This region was selected to complement our earlier assessment of the Tropics, as the North Atlantic exhibits distinct decadal dynamics (Eade et al. 2014). We take a single member at a time from the ArchesClimate ensemble, and determine its pixel-wise rank among the 10-member IPSL-DCPP ensemble. We then average the rank of all ten ArchesClimate members. This gives us many samples to have a clear picture on the interchangeability of the ensemble members generated by ArchesClimate. We utilized the same variable subset as in subsection e. See subsection a for a detailed methodology on rank histograms. The results indicate varying degrees of exchangeability. ArchesClimate produces relatively flat rank histograms for *net_flux* and *wap*, (see Figure 6), suggesting that ArchesClimate members are statistically indistinguishable from IPSL-DCPP members for these variables. However, we observed distinct biases in other areas. ArchesClimate consistently under-predicted values for *tos* and *thetaot2000*, resulting in a rank histogram skewed toward the lowest ranks. In the atmosphere, several variables exhibited n-shaped (convex) histograms, indicating that ArchesClimate members are more likely to rank in the middle of the IPSL-DCPP ensemble. This is consistent with the findings in subsection e, which showed that ArchesClimate generally exhibits lower variance than IPSL-DCPP.

g. Comparison of Temporal Power Spectra

This experiment compares the Temporal Power Spectra (TPS) of both IPSL-DCPP and ArchesClimate to compare signals at different temporal frequencies. We look at the TPS of a 10-year 10-member ensemble initialized at 1969 for the North Atlantic, and take the mean across members. We use anomalies for all variables and use the same variable subset as in subsection c.

In Figure 6, there is a noticeable annual, seasonal and monthly signal for all variables in ArchesClimate. ArchesClimate is over-predicting the annual and seasonal cycle, suggesting that ArchesClimate is memorizing the annual and seasonal cycles. For all variables that have n-shaped rank histograms, ArchesClimate is underpowered in all but the strongest cycles. In *psl* (sea-level pressure), ArchesClimate correctly captures the strong annual cycle but under-represents everywhere else. This gives us insight into where ArchesClimate is unable to capture the variability of certain variables. It is clear in Figure 6 that the variables with lower variance are unable to

generate enough power at frequencies outside of monthly, seasonal and annual cycles. This helps inform how to increase variance by including spectral information in the loss function. We investigate this idea in subsection j.

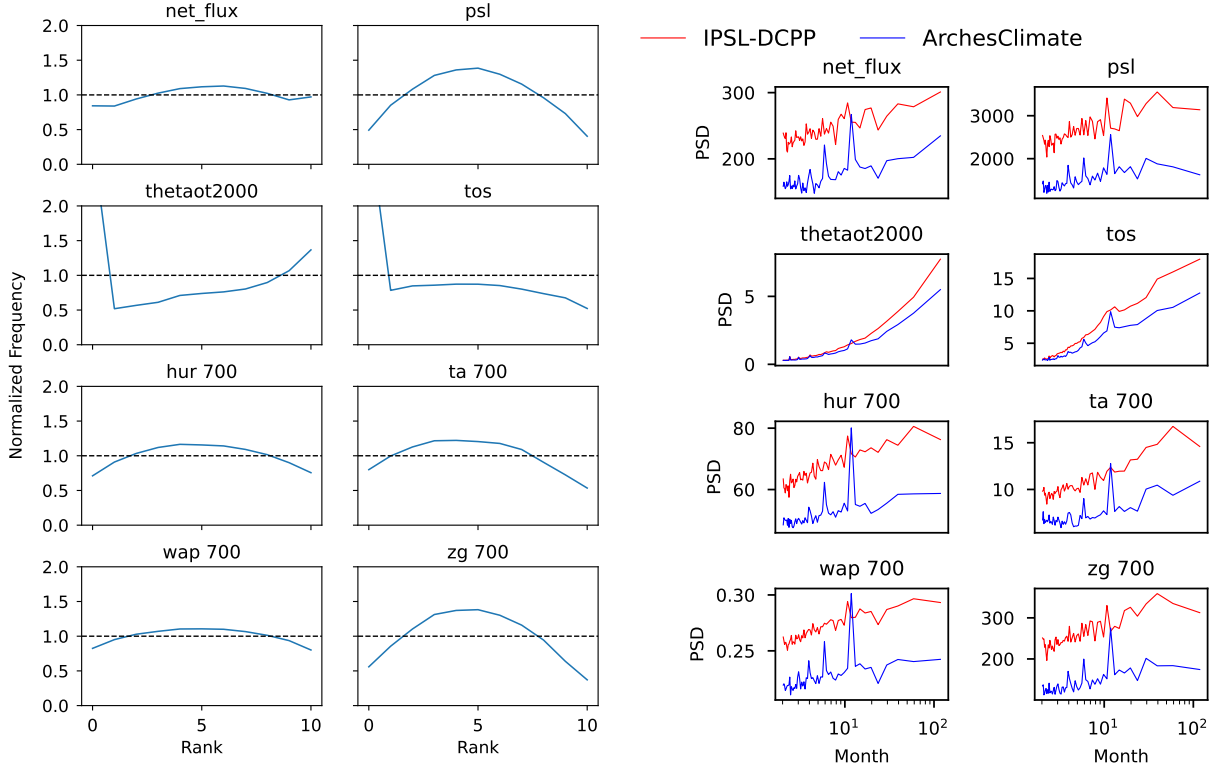


FIG. 6: Diagnostics for the North Atlantic for test period 1969-1979. On the left, rank histograms for ArchesClimate showing normalized frequency of the rank of a each ArchesClimate member in a 10-member ensemble of IPSL-DCPP. Values closer to one indicate better interchangeability with IPSL-DCPP. On the right, comparison of the temporal power spectral density of anomalies of 10-member ensembles across time for ArchesClimate and IPSL-DCPP. The x-axis is logarithmic, with the smallest value being one month.

h. Calculating the Correlation of the Linear Trend

We calculate the correlation of the linear trend to understand how well the ensemble mean of ArchesClimate captures spatial decadal trends of IPSL-DCPP. We calculate the per-pixel correlation of linear trend between different models for sea surface temperature anomalies. We use a 5-member ensemble for the periods 1969-1979, 1979-1989 and 2010-2020 from ArchesClimate. For the same period, we use a 10-member ensemble from IPSL-DCPP, which we split the ensemble into two 5-member ensembles. First we use to compute the correlation of the two 5-member IPSL-DCPP

ensembles (IPSL vs. IPSL in Figure 7). We then compute the correlation of the linear trend of the 5-member ArchesClimate ensemble and one of the 5-member IPSL-DCPP ensembles.

We show in Figure 7 that in regions with strong teleconnections, i.e. the North Atlantic, Pacific, and Indian Ocean, ArchesClimate has similar linear trend over the decade as IPSL-DCPP. The persistence of these correlations in key basins indicates that ArchesClimate retains a similar level of decadal-scale predictive skill as IPSL-DCPP. ArchesClimate decorrelates throughout the decade in the high latitudes much more than IPSL-DCPP. In each of the three test periods, there is a decorrelation near Northern Canada and Greenland. ArchesClimate does not represent any sea-ice or ice dynamics, and is therefore limited in its ability to capture long-term dynamics of Arctic regions. The linear trend in 1979-1989 is less correlated than the other two decades, and is accordingly represented in ArchesClimate.

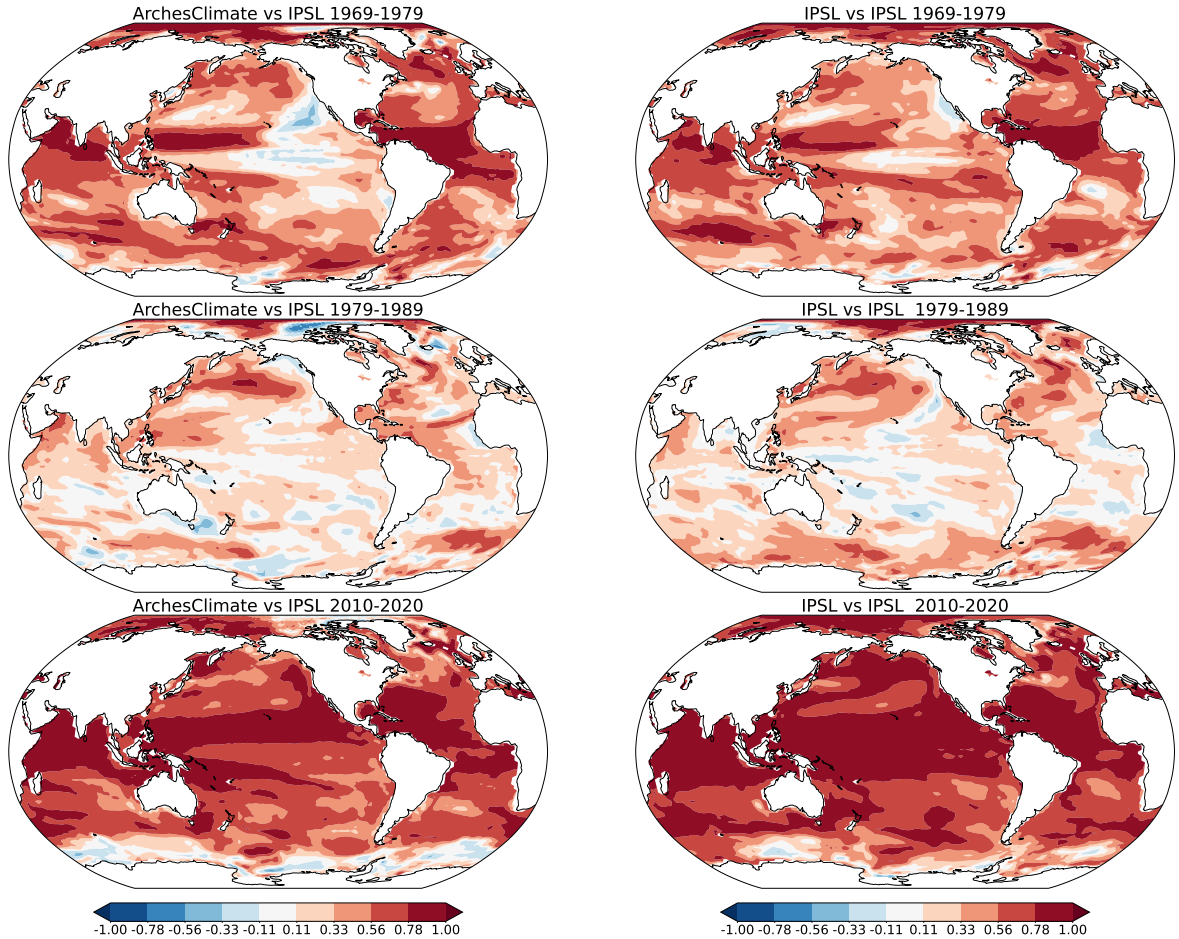


FIG. 7: Correlation of tos (sea surface temperature) anomalies for several periods for both IPSL-DCPP and ArchesClimate. We use the ensemble mean of 5-member ensembles. The correlation calculated by finding the linear trend of the anomalies between IPSL-DCPP and ArchesClimate per pixel over the 10 years. Values closer to one indicate higher correlation.

i. Spatial Anomaly Analysis in the North Atlantic

In previous experiments, we investigated the ability of ArchesClimate to capture regionally and globally averaged patterns (subsection c and subsection e). We look again at the anomalies of sea surface temperature in the North Atlantic, but now to understand how well ArchesClimate captures the spatial signal of the seasonal cycle. We compute averages of seasonal sea surface temperature anomalies for the 10-year test period initialized at 1969 over the North Atlantic (0° – 65° N, 80° – 0° W). The seasonal means are MAM (March, April, May), JJA (June, July, August), SON (September, October, November) and DJF (December, January, February). We compare the results to the baseline outlined in subsection a.

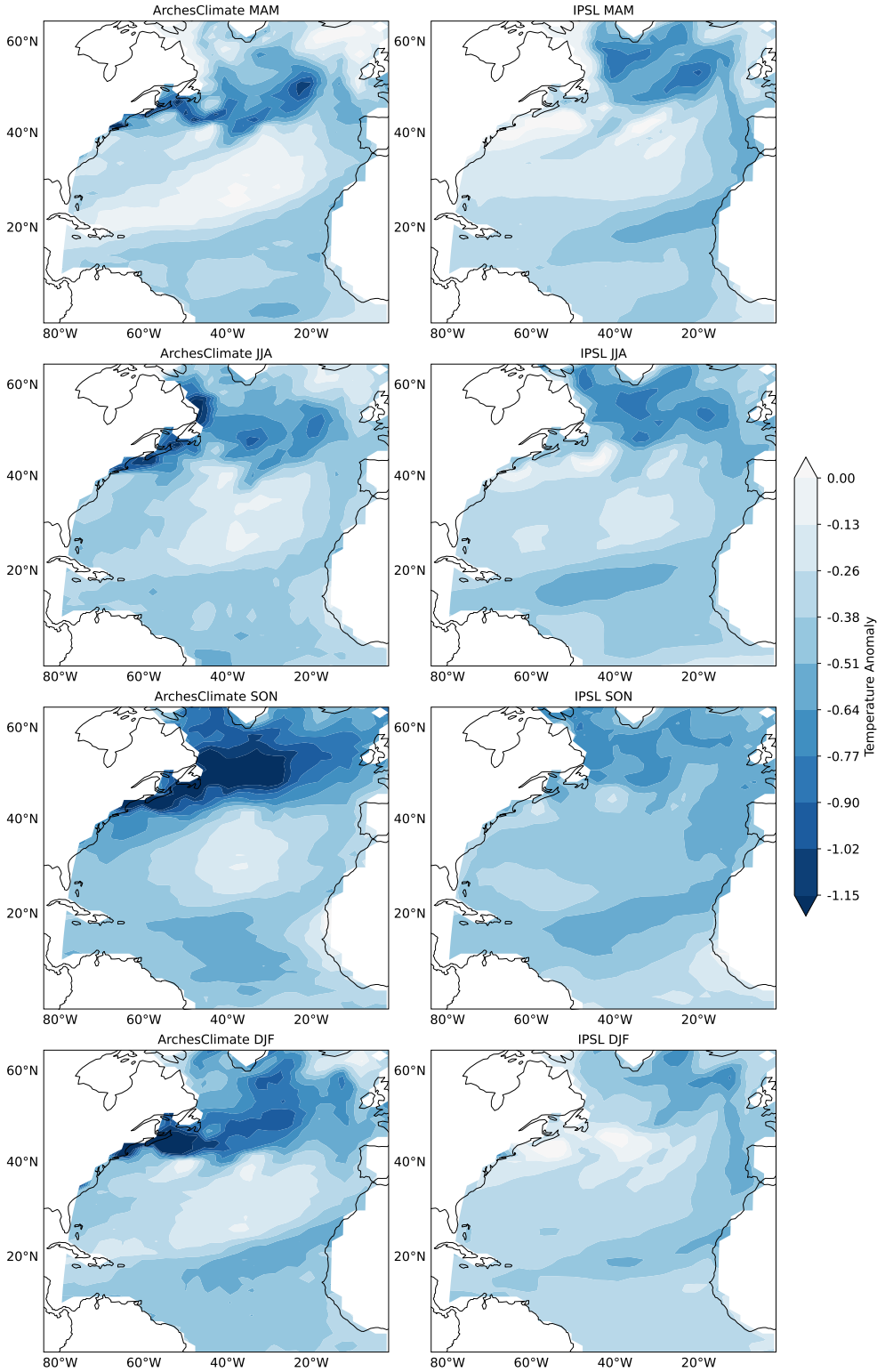


FIG. 8: Averages of seasonal anomalies of sea surface temperature over the North Atlantic (0° – 65° N, 80° – 0° W) for the test period 1969–1979. Here we compare a 5-member ensemble from ArchesClimate to a 5-member ensemble of IPSL-DCPP seasonally averaged over the decade. This complements the statistics shown in subsection e.

We can see that in Figure 8, ArchesClimate captures spatial patterns of the summer seasons. In the winter seasons, ArchesClimate produces colder states than IPSL-DCPP in the northern-most part of the Atlantic. This could be because the effect of the external forcings is much higher in the winter seasons; the mixed layer of the ocean is shallower in the summer months, relating to a weaker effect. In Figure 4, there is no clear indication that there is a bias in the winter seasons and that ArchesClimate can understand on aggregate seasonal patterns of variability.

j. Improving Variance in ArchesClimate

In this experiment, we explore ways to increase the variance lacking in ArchesClimate shown in Table 3. We compare three methods to improve variability. First, we multiply the initial noise at inference time by 1.1 (referred to as *AC_noised*) following ArchesWeatherGen (Couairon et al. 2024). The generative model takes the scaled noise distribution and translates this to a higher variance output distribution. Second, we apply noise scaling proportional to the difference in variance between the generated data and the target data for the validation period for each variable (*AC_per_variable*). Finally, we train another model with a spectral and image gradient loss (*AC_updated_loss*). To balance the weighting of the loss functions, we scale the gradient loss and spectral loss by 0.2. The loss function is as follows:

$$\mathcal{L}_{\text{MSE}} = \mathbb{E} \left[(P_{i,j} - G_{i,j})^2 \right] \quad (7)$$

$$\mathcal{L}_{\text{grad}} = \mathbb{E} \left[\left| (P_{i,j+1} - P_{i,j}) - (G_{i,j+1} - G_{i,j}) \right|^2 \right] + \mathbb{E} \left[\left| (P_{i+1,j} - P_{i,j}) - (G_{i+1,j} - G_{i,j}) \right|^2 \right] \quad (8)$$

$$\mathcal{L}_{\text{PSD}} = \mathbb{E} \left[\left(\log \left(|\mathcal{F}(P)|^2 + \epsilon \right) - \log \left(|\mathcal{F}(G)|^2 + \epsilon \right) \right)^2 \right] \quad (9)$$

$$\mathcal{L}_{\text{total}} = \mathcal{L}_{\text{MSE}} + 0.2 * \mathcal{L}_{\text{grad}} + 0.2 * \mathcal{L}_{\text{PSD}} \quad (10)$$

Where:

P is the prediction and $P_{i,j}$ is the pixel at i, j

G is the ground truth

\mathcal{F} denotes the 2D Fourier transform of the predicted image

$|\mathcal{F}|^2$ denotes the Power Spectra Density

In Figure 9 we can observe that both the noise scaling and per-noise scaling has little effect, and the alternate loss function successfully captures variance in *tos* and *ta* while improving significantly the variance in *psl* previously having low variance. The benefit here is twofold. The extra terms in the alternate loss function encourage ArchesClimate to pay attention more to spatial patterns and make the learning task much more difficult. While this new loss function improves variance in ArchesClimate, it reduces the accuracy of the model. The loss function increases CRPS for several variables, and balancing this tradeoff is left for further research.

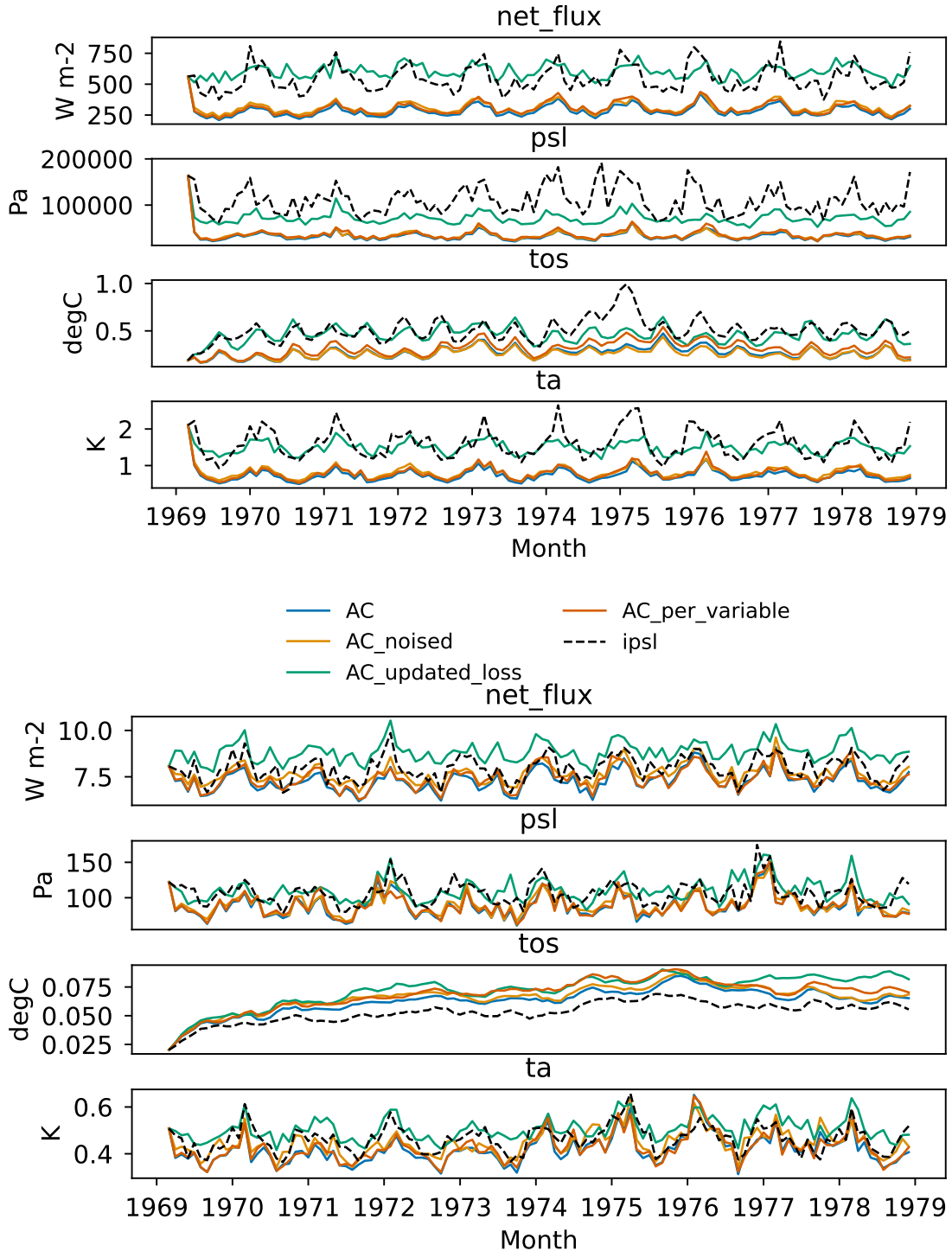


FIG. 9: Variance (top) and CRPS (bottom) of different techniques to increase variance in Arch-esClimate. AC_noised increases initial noise at inference time by a factor of 1.1. AC_updated_loss uses an alternate loss function including gradient and spectral components. AC_per_variable scales the initial noise by the difference of variance in a generated ensemble versus the target ensemble for the test period for each variable. We compare 5-member ensembles for the test period 1969-1979. Values closest to the IPSL-DCPP 5-member ensemble (the dotted black line) are best.

4. Discussion and Conclusions

Our research aims to advance climate modeling by providing an inexpensive tool to generate ensemble members, enabling more robust probabilistic analysis. We propose ArchesClimate and demonstrate its use in generating ensemble members of the IPSL-CM6A-LR by training on climate model outputs and using forcings from *input4mips* to condition our model. We show that a combination of a deterministic and a generative machine learning model (based on ArchesWeatherGen) is an effective way to learn climate dynamics at low computational cost. We also find that the model can autoregressively produce climatically consistent 10-year sequences at a one-month timestep.

We evaluate ArchesClimate using both statistical and physical evaluations and find that it reliably reproduces key features of decadal climate variability. The model captures long-term correlations among ensemble members across regions that drive climate through teleconnections, while also reproducing seasonal spring and summer anomalies in close agreement with IPSL-DCPP. Across oceanic and atmospheric variables, ArchesClimate achieves comparable CRPS performance to IPSL-DCPP over multiple decades and replicates temporal power spectra consistent with major climate signals. Together, these results demonstrate that ArchesClimate is a reasonable approach for studying decadal climate variability.

While we train with data that is the output of a climate model, the model does not receive the initial conditions used to start each ensemble member of IPSL-DCPP. The impact of omitting the initialization state of the climate model is limited, as initialization noise has been shown to fade after a short period (Smith et al. 2019). In ArchesClimate, we create variation between ensemble members by generating states from different samples of Gaussian noise.

We include a holistic climate state in order to improve forecasting accuracy and generate more physically consistent states. In future work, however, possible that ArchesClimate could benefit from a more thorough set of forcings and input variables (e.g. sea ice, land-use). Similarly, a running average of the last decade’s climate could help the model as a sort of memory, especially for variables that operate on longer timescales (Mignot et al. 2016). By better constraining the model through these extra variables, we would expect to produce a more constrained output.

Our objective was to capture the underlying distribution of each physical variable at each timestep so that we can generate samples of the distribution of a given climate while still obeying dynamics that are resolved at shorter timescales. This task is difficult as the target distribution is hidden and

the assessment of samples from the distribution requires expertise in climate science (Mignot et al. 2016). To aid the assessment of samples, we proposed a set of evaluations of both the statistics and the physical properties of the AI-generated ensembles that can be used in future evaluations of probabilistic climate model emulators. Further work can be done to find a base set of metrics and evaluations using already existing tools such as PCMDI, ESMValTool, climpred, and xMIP. With more thorough metrics, we can increase confidence in the ability of climate model emulators to augment climate models. Analyses can also be done to see if the climate model emulator adheres to conservation properties such as hydrostatic constraints and total water in atmospheric columns (Sha et al. 2025; White et al. 2024; Watt-Meyer et al. 2024).

Despite the encouraging results, this work is subject to several key limitations. Primarily, the use of coarse temporal resolution prevents fine-grained analysis of high-frequency climate phenomena. This modeling choice was motivated by the higher predictability of low-frequency phenomena, and the computational gains of predicting climate states at a monthly temporal resolution. Furthermore, ArchesClimate directly inherits any inherent biases present in the underlying climate model, IPSL-CM6A-LR. A significant technical constraint observed is the underprediction of variance across several critical variables, which may limit the model’s ability to capture extreme events. Additionally, the variable set is limited and contains a restricted representation of ocean variables, thereby constraining the scope of oceanic climate interactions that can be studied. We trained a single model on a short time period that contained a large amount of data to better evaluate the model’s learning limits. Finally, the ability to conduct comprehensive model ablations and hyperparameter sensitivity analyses was constrained by the high computational resource requirements necessary for training and evaluation.

Our work opens several new directions of research. Using members generated from ArchesClimate, we believe it will be possible to temporally and spatially downscale using similar generative methods to enable analysis at higher resolutions. Further work also includes training on longer experiments such as the Coupled Model Inter-comparison Project experiment *historical* simulations that span several hundred years. By extending ArchesClimate to multi-decadal climate simulations, we can assess if it can emulate inter-annual variability at long timescales (Jain et al. 2023). Expanding the forcings already used in ArchesClimate, interpolation between longer experiments can be investigated to help climate scientists explore previously untested future climate scenarios.

Another possibility is to explore recent advances in generative methods, for which inference time can be done in a fraction of the time, sometimes using only a single inference step (Hess et al. 2025; Schmitt et al. 2024), which would cut the cost of generating samples by an order of magnitude. Our short investigation into the ability of ArchesClimate to stably generate states for longer temporal periods (see Appendix A2 suggest that emulating climate states at a monthly resolution is an efficient way to predict long-term climate dynamics. Further work is needed to explore the limits of jointly predicting multiple dynamics at monthly time scales. It remains an open question whether ArchesClimate is primarily capturing the underlying processes that operate at shorter timescales, or whether some of its skill at monthly prediction may arise from correlations present at those scales.

ArchesClimate offers a powerful and efficient complement to traditional climate modeling approaches. By leveraging machine learning, ArchesClimate produces decadal climate predictions with comparable accuracy at a fraction of the computational cost of running a climate model. This advancement enables broader access to probabilistic climate projections and supports more timely, informed decision-making in response to climate change.

APPENDIX

A1. Derivation of *net_flux*

This is a derivation of the variable *net_flux* that is used in ArchesClimate. We define *net_flux* as:

$$net_flux = rsus - rsds + rlus - rlds + hfss + hfsls \quad (A1)$$

rsus Surface Upwelling Shortwave Radiation

rsds Surface Downwelling Shortwave Radiation

rlus Surface Upwelling Longwave Radiation

rlds Surface Downwelling Longwave Radiation

hfss Surface Upward Sensible Heat Flux

hfsls Surface Upward Latent Heat Flux

A2. Long-term Forcing Response

We generate states for 50 years to test the ability of ArchesClimate to respond to external forcings and remain stable over 50 years. We compare these states to generated states that are conditioned with forcings for the year 1969 are repeated every year for 50 years. We take the first ensemble of the validation period (the ensemble initialized at 1969) and the first ensemble of the test period (the ensemble initialized at 2010) to mark the beginning and the end of the 50-year rollout.

Figure A1 shows the results for sea surface temperature, where ArchesClimate is much closer to the trend of the dataset than the rollout with repeated forcings. Even with limited forcings, there is a noticeable effect on sea surface temperature. By expanding the scope of the forcings, we may be able to capture more complex long-term dynamics.

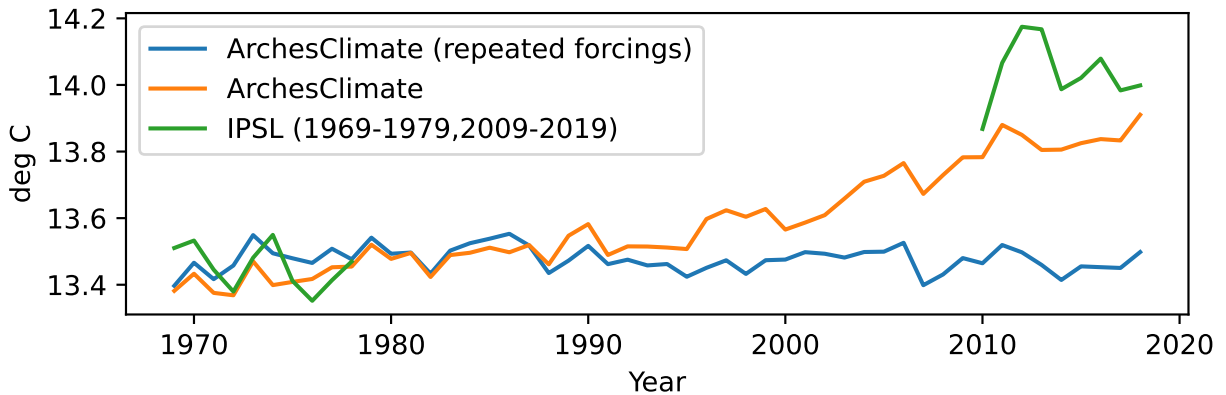


FIG. A1: Yearly means of a 50-year rollout of ArchesClimate with and without constant forcings for *tos* (sea surface temperature). Two IPSL-DCPP decades are used for reference.

A3. Alternative Train/Test Splits

In the train/test split of IPSL-DCPP described in subsection d, there is temporal overlap in the training and test sets. Here, we look at a train/test split that leaves a test set temporally apart from the train set. To do this, we use the initialization years 1960-2000, so the last year of training is 2009, which we refer to in Figure A2 as *alternative*. We can then compare a model that has seen the years 2010-2020 to a model that has not. We generate a 10-member ensemble initialized in 2010 for both models.

We compare CRPS in Figure A2. There is a noticeable difference in CRPS between ArchesClimate and IPSL-DCPP for the variables *tos* and *ta* towards the end of the decade. ArchesClimate

performs much better when it has seen samples from the period of generation. Further investigation is needed to understand if a more comprehensive set of external forcings will improve the ability of ArchesClimate to extrapolate to unseen futures. We use the original train/test split for several reasons: our goal in this research is to augment the IPSL-CM6A-LR and not to extend the dataset beyond its current period. As well, the current train/test split allows for temporal comparison throughout the dataset, providing a more thorough analysis.

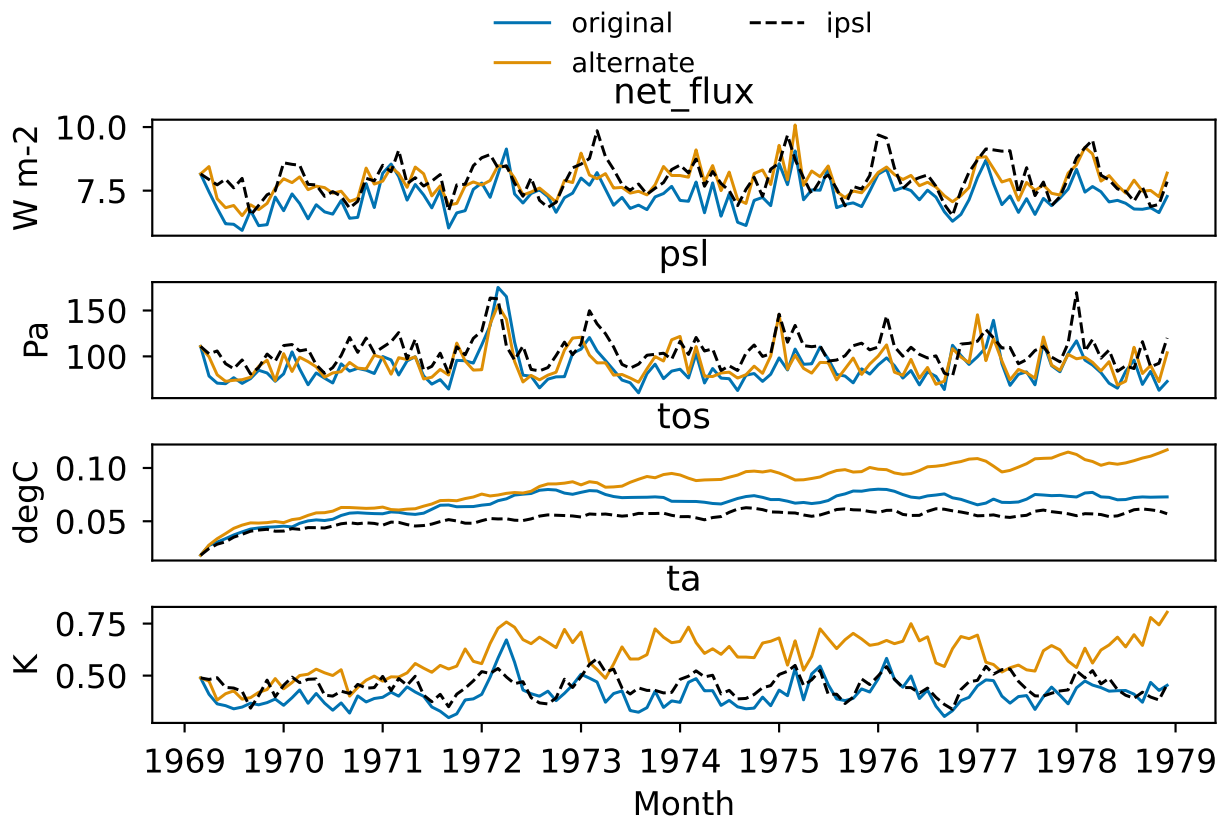


FIG. A2: Comparison of CRPS for different train/test splits. “original” indicates the training scheme outlined in subsection d and “alternative” indicates the training scheme where training and test contain no temporal overlap. Better values are closer to the dotted line, which is the 5-member IPSL-DCPP baseline. We compare 5-member ensembles for the test period 1969-1979.

Acknowledgments. G. Clyne, G. Couairon, and C. Monteleoni were primarily supported by the Choose France Chair in AI, from the French government. The authors thank Juliette Mignot, David Landry, Clément Dauvilliers, and Renu Singh for several discussions about the project. To process the data from IPSL, this study benefited from the IPSL mesocenter ESPRI facility, which is supported by CNRS, UPMC, Labex L-IPSL, CNES and Ecole Polytechnique.

Data availability statement. Code for the project can be found at <https://github.com/INRIA/geoarches>. The dataset used for training can be found at <https://esgf-node.ipsl.upmc.fr/projects/cmip6-ipsl/>.

References

- Acosta, M. C., and Coauthors, 2024: The computational and energy cost of simulation and storage for climate science: Lessons from CMIP6. *Geoscientific Model Development*, **17** (8), 3081–3098, <https://doi.org/10.5194/gmd-17-3081-2024>.
- Bi, K., L. Xie, H. Zhang, X. Chen, X. Gu, and Q. Tian, 2022: arXiv:2211.02556. Pangu-Weather: A 3D High-Resolution Model for Fast and Accurate Global Weather Forecast. arXiv, 2211.02556.
- Boer, G. J., and Coauthors, 2016: The Decadal Climate Prediction Project (DCPP) contribution to CMIP6. *Geoscientific Model Development*, **9** (10), 3751–3777, <https://doi.org/10.5194/gmd-9-3751-2016>.
- Boucher, O., and Coauthors, 2020: Presentation and Evaluation of the IPSL-CM6A-LR Climate Model. *Journal of Advances in Modeling Earth Systems*, **12** (7), e2019MS002010, <https://doi.org/10.1029/2019MS002010>.
- Brenowitz, N. D., and Coauthors, 2025: arXiv:2505.06474. Climate in a Bottle: Towards a Generative Foundation Model for the Kilometer-Scale Global Atmosphere. arXiv, <https://doi.org/10.48550/arXiv.2505.06474>, 2505.06474.
- Cachay, S. R., B. Zhao, H. Joren, and R. Yu, 2023: arXiv:2306.01984. DYffusion: A Dynamics-informed Diffusion Model for Spatiotemporal Forecasting. arXiv, 2306.01984.

- Chen, M., X. Tan, B. Li, Y. Liu, T. Qin, S. Zhao, and T.-Y. Liu, 2021: arXiv:2103.00993. AdaSpeech: Adaptive Text to Speech for Custom Voice. arXiv, <https://doi.org/10.48550/arXiv.2103.00993>, 2103.00993.
- Clark, S. K., and Coauthors, 2024: arXiv:2412.04418. ACE2-SOM: Coupling an ML atmospheric emulator to a slab ocean and learning the sensitivity of climate to changed CO₂. arXiv, <https://doi.org/10.48550/arXiv.2412.04418>, 2412.04418.
- Couairon, G., R. Singh, A. Charantonis, C. Lessig, and C. Monteleoni, 2024: arXiv:2412.12971. ArchesWeather & ArchesWeatherGen: A deterministic and generative model for efficient ML weather forecasting. arXiv, <https://doi.org/10.48550/arXiv.2412.12971>, 2412.12971.
- Cresswell-Clay, N., B. Liu, D. Durran, Z. Liu, Z. I. Espinosa, R. Moreno, and M. Karlbauer, 2025: arXiv:2409.16247. A Deep Learning Earth System Model for Efficient Simulation of the Observed Climate. arXiv, <https://doi.org/10.48550/arXiv.2409.16247>, 2409.16247.
- Deser, C., W. M. Kim, R. C. J. Wills, I. R. Simpson, S. Yeager, G. Danabasoglu, K. Rodgers, and N. Rosenbloom, 2024: Effects of macro vs. micro initialization and ocean initial-condition memory on the evolution of ensemble spread in the CESM2 large ensemble. *Climate Dynamics*, **63** (1), 62, <https://doi.org/10.1007/s00382-024-07553-z>.
- Dheeshjith, S., A. Subel, A. Adcroft, J. Busecke, C. Fernandez-Granda, S. Gupta, and L. Zanna, 2025: arXiv:2412.03795. Samudra: An AI Global Ocean Emulator for Climate. arXiv, <https://doi.org/10.48550/arXiv.2412.03795>, 2412.03795.
- Duncan, J. P. C., and Coauthors, 2025: arXiv:2509.12490. SamudrACE: Fast and Accurate Coupled Climate Modeling with 3D Ocean and Atmosphere Emulators. arXiv, <https://doi.org/10.48550/arXiv.2509.12490>, 2509.12490.
- Eade, R., D. Smith, A. Scaife, E. Wallace, N. Dunstone, L. Hermanson, and N. Robinson, 2014: Do seasonal-to-decadal climate predictions underestimate the predictability of the real world? *Geophysical Research Letters*, **41** (15), 5620–5628, <https://doi.org/10.1002/2014GL061146>.
- Esser, P., and Coauthors, 2024: arXiv:2403.03206. Scaling Rectified Flow Transformers for High-Resolution Image Synthesis. arXiv, <https://doi.org/10.48550/arXiv.2403.03206>, 2403.03206.

- Estella-Perez, V., J. Mignot, E. Guilyardi, D. Swingedouw, and G. Reverdin, 2020: Advances in reconstructing the AMOC using sea surface observations of salinity. *Climate Dynamics*, **55** (3), 975–992, <https://doi.org/10.1007/s00382-020-05304-4>.
- Fischer, E. M., and Coauthors, 2023: Storylines for unprecedented heatwaves based on ensemble boosting. *Nature Communications*, **14** (1), 4643, <https://doi.org/10.1038/s41467-023-40112-4>.
- Fyfe, J. C., and Coauthors, 2017: Large near-term projected snowpack loss over the western United States. *Nature Communications*, **8** (1), 14996, <https://doi.org/10.1038/ncomms14996>.
- Guan, H., T. Arcomano, A. Chattopadhyay, and R. Maulik, 2024: arXiv:2405.16297. LUCIE: A Lightweight Uncoupled Climate Emulator with long-term stability and physical consistency for O(1000)-member ensembles. arXiv, <https://doi.org/10.48550/arXiv.2405.16297>, 2405.16297.
- Hamill, T. M., 2001: Interpretation of Rank Histograms for Verifying Ensemble Forecasts.
- Hasselmann, K., 1976: Stochastic climate models Part I. Theory. *Tellus*, **28** (6), 473–485, <https://doi.org/10.1111/j.2153-3490.1976.tb00696.x>.
- Held, I. M., M. Winton, K. Takahashi, T. Delworth, F. Zeng, and G. K. Vallis, 2010: Probing the Fast and Slow Components of Global Warming by Returning Abruptly to Preindustrial Forcing. *Journal of Climate*, **23** (9), 2418–2427, <https://doi.org/10.1175/2009JCLI3466.1>.
- Hess, P., M. Aich, B. Pan, and N. Boers, 2025: Fast, scale-adaptive and uncertainty-aware downscaling of Earth system model fields with generative machine learning. *Nature Machine Intelligence*, **7** (3), 363–373, <https://doi.org/10.1038/s42256-025-00980-5>.
- Ho, J., N. Kalchbrenner, D. Weissenborn, and T. Salimans, 2019: arXiv:1912.12180. Axial Attention in Multidimensional Transformers. arXiv, <https://doi.org/10.48550/arXiv.1912.12180>, 1912.12180.
- Jain, S., A. A. Scaife, T. G. Shepherd, C. Deser, N. Dunstone, G. A. Schmidt, K. E. Trenberth, and T. Turkington, 2023: Importance of internal variability for climate model assessment. *npj Climate and Atmospheric Science*, **6** (1), 68, <https://doi.org/10.1038/s41612-023-00389-0>.

- Kim, J. Y., J.-S. Kang, and M. Joh, 2021: GPU acceleration of MPAS microphysics WSM6 using OpenACC directives: Performance and verification. *Computers & Geosciences*, **146**, 104627, <https://doi.org/10.1016/j.cageo.2020.104627>.
- Kochkov, D., and Coauthors, 2024: arXiv:2311.07222. Neural General Circulation Models for Weather and Climate. arXiv, 2311.07222.
- Lipman, Y., R. T. Q. Chen, H. Ben-Hamu, M. Nickel, and M. Le, 2023: arXiv:2210.02747. Flow Matching for Generative Modeling. arXiv, 2210.02747.
- Liu, Z., Y. Lin, Y. Cao, H. Hu, Y. Wei, Z. Zhang, S. Lin, and B. Guo, 2021: arXiv:2103.14030. Swin Transformer: Hierarchical Vision Transformer using Shifted Windows. arXiv, 2103.14030.
- Lurton, T., and Coauthors, 2020: Implementation of the CMIP6 Forcing Data in the IPSL-CM6A-LR Model. *Journal of Advances in Modeling Earth Systems*, **12** (4), e2019MS001940, <https://doi.org/10.1029/2019MS001940>.
- Maher, N., S. Milinski, and R. Ludwig, 2021: Large ensemble climate model simulations: Introduction, overview, and future prospects for utilising multiple types of large ensemble. *Earth System Dynamics*, **12** (2), 401–418, <https://doi.org/10.5194/esd-12-401-2021>.
- Meinshausen, M., and Z. R. J. Nicholls, 2018: UoM-AIM-ssp370-1-2-1 GHG concentrations. Earth System Grid Federation. doi:<https://doi.org/10.22033/ESGF/input4MIPs.9861> . Earth System Grid Federation.
- Mignot, J., J. García-Serrano, D. Swingedouw, A. Germe, S. Nguyen, P. Ortega, E. Guilyardi, and S. Ray, 2016: Decadal prediction skill in the ocean with surface nudging in the IPSL-CM5A-LR climate model. *Climate Dynamics*, **47** (3-4), 1225–1246, <https://doi.org/10.1007/s00382-015-2898-1>.
- Rasp, S., and Coauthors, 2024: arXiv:2308.15560. WeatherBench 2: A benchmark for the next generation of data-driven global weather models. arXiv, <https://doi.org/10.48550/arXiv.2308.15560>, 2308.15560.
- Schmitt, M., V. Pratz, U. Köthe, P.-C. Bürkner, and S. T. Radev, 2024: arXiv:2312.05440. Consistency Models for Scalable and Fast Simulation-Based Inference. arXiv, <https://doi.org/10.48550/arXiv.2312.05440>, 2312.05440.

- Servonnat, J., J. Mignot, E. Guilyardi, D. Swingedouw, R. Séférian, and S. Labetoulle, 2015: Reconstructing the subsurface ocean decadal variability using surface nudging in a perfect model framework. *Climate Dynamics*, **44** (1), 315–338, <https://doi.org/10.1007/s00382-014-2184-7>.
- Sha, Y., J. S. Schreck, W. Chapman, and D. J. G. II, 2025: arXiv:2501.05648. Improving AI weather prediction models using global mass and energy conservation schemes. arXiv, <https://doi.org/10.48550/arXiv.2501.05648>, 2501.05648.
- Smith, D. M., and Coauthors, 2019: Robust skill of decadal climate predictions. *npj Climate and Atmospheric Science*, **2** (1), 1–10, <https://doi.org/10.1038/s41612-019-0071-y>.
- Tebaldi, C., and J. M. Arblaster, 2014: Pattern scaling: Its strengths and limitations, and an update on the latest model simulations. *Climatic Change*, **122** (3), 459–471, <https://doi.org/10.1007/s10584-013-1032-9>.
- Vaswani, A., N. Shazeer, N. Parmar, J. Uszkoreit, L. Jones, A. N. Gomez, L. ukasz Kaiser, and I. Polosukhin, 2017: Attention is All you Need. *Advances in Neural Information Processing Systems*, Curran Associates, Inc., Vol. 30.
- Wang, C., 2019: Three-ocean interactions and climate variability: A review and perspective. *Climate Dynamics*, **53** (7), 5119–5136, <https://doi.org/10.1007/s00382-019-04930-x>.
- Watson-Parris, D., and Coauthors, 2022: ClimateBench v1.0: A Benchmark for Data-Driven Climate Projections. *Journal of Advances in Modeling Earth Systems*, **14** (10), <https://doi.org/10.1029/2021MS002954>.
- Watt-Meyer, O., and Coauthors, 2023: arXiv:2310.02074. ACE: A fast, skillful learned global atmospheric model for climate prediction. arXiv, 2310.02074.
- Watt-Meyer, O., and Coauthors, 2024: arXiv:2411.11268. ACE2: Accurately learning subseasonal to decadal atmospheric variability and forced responses. arXiv, <https://doi.org/10.48550/arXiv.2411.11268>, 2411.11268.
- White, A., A. Büttner, M. Gelbrecht, V. Duruisseaux, N. Kilbertus, F. Hellmann, and N. Boers, 2024: arXiv:2410.23667. Projected Neural Differential Equations for Learning Constrained Dynamics. arXiv, <https://doi.org/10.48550/arXiv.2410.23667>, 2410.23667.